



# Particle breakage and morphology changes of calcareous sands under one-dimensional compression loading

Houzhen Wei<sup>1</sup> · Hao Liu<sup>1,2,3</sup> · Tao Zhao<sup>4</sup> · Shudong Zhang<sup>4</sup> · Linjian Ma<sup>5</sup> · Mei Yin<sup>4</sup> · Qingshan Meng<sup>1</sup>

Received: 8 July 2022 / Accepted: 10 November 2022  
© The Author(s) 2022

## Abstract

Particle breakage and the corresponding change of morphology are two key factors governing the mechanical behavior of calcareous sands in offshore geotechnical engineering constructions. To reveal the characteristics of these two factors, oedometer tests on calcareous sands have been performed in this study. The materials were sampled from the South China Sea with a homogenous composition but different particle size ranges and relative densities. In these tests, the dynamic imaging analysis (DIA) by Microtrac PartAn<sup>3D</sup> and acoustic emission (AE) techniques were employed to investigate the evolution of particle morphology and characteristics of AE signaling associated with the material deformations, respectively. The compressive deformation of calcareous sands was mainly induced by the particle rearrangement and particle breakage which are effectively irreversible plastic deformations. The irregular particle shape has led to strong interparticle filling and interlocking effects, which affected the particle slippage and rearrangement significantly during the deformation. The intensity and type of AE-triggering micro-mechanical behaviors were characterized by AE ringdown counts (RDC) and peak frequency, respectively. The RDC values concentrated primarily in the compression stage and increased rapidly under the normal stress of 400–3200 kPa. The RDC values increased with the increase of particle size but decreased with the increase of initial relative density. The compressive deformation and breakage characteristics of calcareous sands are consistent with the existing acoustic emission laws.

**Keywords** Calcareous sand · Acoustic emission · One-dimensional compression · Particle breakage

## Introduction

Calcareous sands are widely distributed in shallow tropical and sub-tropical marine environments, such as the Bass

Strait, the Persian Gulf, the Red Sea, the South China Sea, Hawaiian Islands, the continental shelf of Australia, India and Saudi Arabia (Alba and Audibert 1999; He et al. 2021; Liu et al. 2018; McClelland 1988; Murff 1987). Because of their regional distribution, they have been used as the foundation materials of many coastal infrastructures such as embankments, seawalls and offshore piles (Coop et al. 2004; Xiao, Wang, et al. 2019). However, the special composition and unique geological origin give the calcareous sands the characteristics of well-developed internal pore space, irregular shape, and high brittleness, which make their mechanical properties dramatically different from the typical terrigenous sands (El Aal and Nabawy 2019; Miao and Airey 2013; Nabawy et al. 2020; Wei et al. 2021; Xiao and Liu 2017). The lack of adequate understanding the mechanical behavior of calcareous sands during design and construction could potentially lead to unstable or even failure of offshore and costal projects (Brandes 2011; He et al. 2021; Randolph and Gourvenec 2017; Wang et al. 2019; Zhang et al. 2014). In particular, the deformation of

✉ Shudong Zhang  
shudong.zhang@outlook.com

<sup>1</sup> State Key Laboratory of Geomechanics and Geotechnical Engineering, Institute of Rock and Soil Mechanics, Chinese Academy of Sciences, 430071 Wuhan, China  
<sup>2</sup> College of Civil Engineering and Architecture, Guilin University of Technology, 541004 Guilin, China  
<sup>3</sup> Guangxi Key Laboratory of Geomechanics and Geotechnical Engineering, Guilin University of Technology, 541004 Guilin, China  
<sup>4</sup> Department of Civil and Environmental Engineering, College of Engineering, Brunel University London, Uxbridge, UK  
<sup>5</sup> State Key Laboratory of Disaster Prevention & Mitigation of Explosion & Impact, Army Engineering University of PLA, 210007 Nanjing, China

calcareous sands under normal loading is directly related to these engineering practices.

As reported in the literature, the compression of granular material leads to the change of internal structure, during which the interlocking and friction between the particles become increasingly intense (Mesri and Vardhanabhuti 2009). In the meantime, the strong particle interactions at the particle contacts during sliding and rotation can induce particle breakage, which can break the balance of the interlocking state, thereby reducing the strength of the granular assembly. In microscale, particles can break in modes of splitting, explosion, explosive-splitting and chipping, as observed from high-speed microphotographic technology (Wang and Coop 2016). In general, the strength of explosive particle was higher than the other modes. Considering the effects of particle morphology, the sands with high local roundness are normally break in an explosive mode, whereas the particles with low values tend to split.

The particle breakage also controls the soil compressibility and affects the macroscopic mechanical behavior to a considerable extent (Bandini and Coop 2011; Hyodo et al. 2017; Li et al. 2013; Mun and McCartney 2017; Nabawy and El Aal 2019; Uygur and Doven 2006; Xiao et al. 2014; Xiao, Sun, et al. 2019; Yu 2018). It can be encountered in various geotechnical practices, such as the constructions of large slopes, dams or embankments (Sadrekarimi 2012), and piling (Jardine et al. 2013). Under external loading, the breakage of particles during compression or shearing will produce a large portion of fines in the internal voids and subsequently change the particle size distribution (PSD) (Casini et al. 2013). The changes in PSD and packing density eventually have a great impact on the peak friction angle, compressibility, permeability, and the location of the critical state line (CSL) (Bandini and Coop 2011; Manso et al. 2018; Wood and Maeda 2008; Yu 2017). Both laboratory works (Altuhafi and Coop 2011; Pino and Baudet 2015; Xiao, Yuan, et al. 2019) and numerical modelling by discrete element method (DEM) (Ma, Zhou, Chang, et al. 2014; Shi et al. 2016) have shown the initiation and propagation of particle breakages during compressions. Its role in the mechanical behavior of soil has been intensively investigated and characterized (Ma, Zhou and Chang 2014). Particle breakage is mainly affected by the intrinsic material characteristics (e.g., particle shape, mineralogy, particle size), and experimental conditions (e.g., void ratio, relative density, stress level, stress path, loading rate and time) (Wils et al. 2015; Wood and Maeda 2008; Yao et al. 2022). Since particle breakage is a result of the multi-level interactions between these influencing factors, the exact breakage mechanisms and effects on the material strength are extremely complicated (Coop et al. 2004; Wang et al. 2020; Wu et al. 2020). As a type of highly brittle material, calcareous

sands can be easily crushed at even low confining stresses (Ata et al. 2018; Salem et al. 2013; Xiao et al. 2017). Therefore, understanding the mechanisms of particle breakage is highly important for a comprehensive understanding of the mechanical behavior of calcareous sands.

To test the particle breakage behavior of granular materials, the oedometer tests have been widely employed by geotechnical engineers (Miao and Airey 2013). The material exhibits quasi-elastic behavior under low normal loading stresses, while the void ratio decreases rapidly with the increase of the loading pressure. This post-elastic behaviour is usually described as the “yielding” of the granular media (McDowell 2002). As a critical parameter controlling the ground settlement in geotechnical engineering, the yielding stress is the minimum stress for triggering the successive particle breakage (Karatzas et al. 2019; McDowell et al. 1996; Nakata, Kato, et al. 2001). Hardin (1987) presented a stress-strain model for one-dimensional normal strain in cohesionless soils (including sands, gravels, rockfill-like materials etc.) and defined the yielding stress as the normal stress corresponding to the point at which the slope of the reciprocal of void ratio versus stress raised to a power curve began to show a non-linear change. This was then referred to as the “breakpoint” stress and the non-linear change was attributed to the onset of particle breakage. Specimens with better gradation and more angular shapes were found to exhibit smaller “breakpoint” stress values. Coop and Lee (1992) observed that the reduction of soil stiffness under one-dimensional compression and believed that this behavior was caused by the onset of particle breakage. They concluded that the yielding stress was related to the relative density and strength of sand particles. Besides, many other studies have suggested that “yielding” occurred at the moment when the stiffness started to change due to the occurrence of particle breakage (Bolton and Cheng 2002; Kikumoto et al. 2010; Luzzani and MR 2002; McDowell and Bolton 1998; McDowell et al. 1996; McDowell and Harireche 2002; Nakata, Hyodo, et al. 2001; Nakata, Kato, et al. 2001; Russell and Khalili 2004; Wood and Maeda 2008). However, McDowell (2002) argued that the PSD of the specimen at “yielding” has already been changed when compared to its initial state, indicating that that apparent particle breakages could occur under a relatively low normal stress before “yielding”. In addition, the yielding stress increases with the decrease of particle size (McDowell and Amon 2000; Nakata, Kato, et al. 2001) and the increase of initial relative density (Hagerty et al. 1993; Karatzas et al. 2019).

To date, there are limited studies on the effects of particle size and relative density on the compression behavior of calcareous sand (Xu et al. 2020). The quantification of particle breakage is traditionally through the sieving

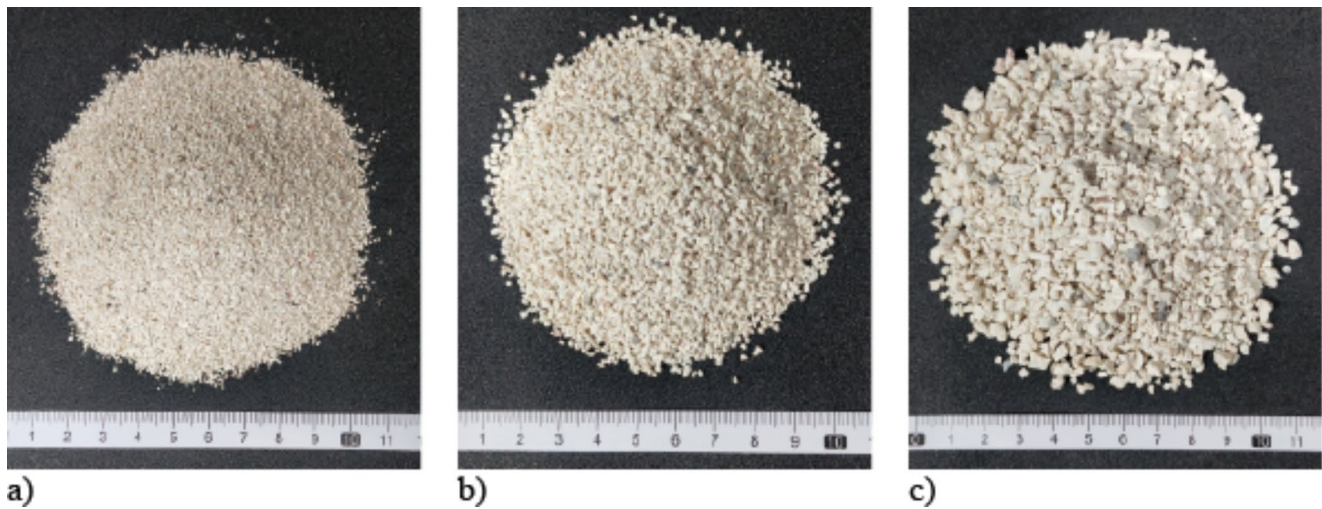


**Fig. 1** Calcareous sands of different particle gradings: **(a)** 0.5–1 mm, **(b)** 1–2 mm, **(c)** 2–5 mm

**Table 1** The physical parameters of calcareous sands

Particle size, $d$ (mm)	Specific gravity, $G_s$	Maximum dry unit weight, $\gamma_{d,max}$ (g/cm <sup>3</sup> )	Minimum dry unit weight, $\gamma_{d,min}$ (g/cm <sup>3</sup> )	The coefficient of uniformity, $C_u$
0.5–1	2.85	1.33	1.08	2.47
1–2	2.85	1.32	1.04	1.59
2–5	2.87	1.32	1.03	1.95

analysis before and after the experiments, which is not accurate when explicit consideration of all particle size ranges is required (Karatza et al. 2019). In this study, to investigate the evolution of particle breakage and the influence of particle size and initial relative density on the mechanical behavior of calcareous sands, a series of oedometer tests were performed at various stress levels. During the experiments, an acoustic emission (AE) system was employed to monitor the AE signals generated by sand breakages. Before and after the experiments, a dynamic image analysis system was employed to characterize and quantify the change of particle morphology. Thereafter, the relationship between particle breakage and statistical characteristics of sands was analyzed. The research could provide new insights into an in-depth understanding of the mechanical properties of calcareous sands, as well as to reveal the influence of the particle morphology on the deformation characteristics of calcareous sands.

## Experimental configuration

### Material and equipment

The calcareous sands used in this study were sampled from an island in the South China Sea. The original sands were

first washed by pure water to remove the fine impurities attached to their surfaces. Then, the sands were dried and sieved. Particles of three different particle size ranges (e.g., 0.5–1 mm, 1–2 mm and 2–5 mm) were selected for the tests (see Fig. 1). The fundamental physical parameters of calcareous sands are shown in Table 1. Since the coefficient of uniformity of all the samples were less than 6, they were classified as poorly graded according to the unified soil classification system (ASTM 2018). The mineral compositions were mainly aragonite, dolomite, and calcite. The XRD (X-ray diffraction) analysis shows that it is mainly composed of calcium carbonate and magnesium carbonate with the weight percentages of 81.08 and 11.55, respectively (Wei et al. 2021). To analyze the particle shape effect, the Microtrac PartAn<sup>3D</sup> Maxi large particle size and shape analyzer (Montgomeryville, Pennsylvania) has been used to scan the individual particles before and after the tests, and then analyzed the particle morphologies via the dynamic image analysis (Wei et al. 2020).

The testing equipment includes the compression system, the dynamic image analysis (DIA) device and the acoustic emission monitoring system. The compression system is a high-pressure oedometer (model: WG-Triple high-pressure single lever arm oedometer) produced by Nanjing Ningxi Soil Instrument Co., Ltd (Nanjing Ningxi Soil Instrument Co., Ltd 2022), which monitored the loading stress and displacement in real time during the test. The soil sample has the diameter of 61.8 mm and thickness of 20 mm. The maximum axial load has the capacity to reach 7,200 kPa. A dial gauge with an accuracy of 0.001 mm was placed on the top of the testing system to monitor the vertical deformation of the sample. The DIA device includes a Microtrac PartAn<sup>3D</sup> Maxi large particle size and shape analyzer (Microtrac 2022). It was used to obtain the morphological parameters of each individual sand particle before and after

**Table 2** AE acquisition system setting parameters

Sampling rate	5 MSPS	Preamplifier gain	40 dB
Recording length	5 K	Detection threshold	40 dB

the tests. It can measure particle ranging in size from 0.16 to 135 mm. More than 40 morphological parameters including size, shape, surface roughness can be characterized in one fast analysis. The AE monitoring system is the model Express-8 AE System manufactured by MISTRAS Group, Inc. (MISTRAS Group, Inc. 2022). The frequency range of the analog filter was set to be between 100 and 400 kHz and the sampling rate was 5 MSPS (Mega Samples Per Second) (the higher the sampling frequency, the more realistic the acoustic wave shape). During the tests, the AE activities were monitored in real time and the AE events could be automatically captured.

### Experimental configurations

Oedometer tests with loading and unloading cycles were carried out on calcareous sands. The loading pressures were set as 12.5, 25, 50, 100, 200, 300, 400, 800, 1600, 2400, 3200, 4000, 4800, 5600, 6400, 7200 kPa at different stages. The sample displacement measured by the dial gauge was recorded before each loading stage and at every hour after the load was applied. When the difference between the two successive readings became less than 0.01 mm, the deformation of the sample was considered to be stable. Then, the next level of pressure could be applied. The unloading path was set in a descending order opposite to the loading path. To improve the uniformity and reduce the testing uncertainty, the specimens were prepared by slowly air pluviating sands in three layers into the sample container. Each layer of sands should be smoothed over as much as possible after been poured into the container. The initial relative density ( $D_r$ ) of the sample was set as 50%, 55%, 60%, 65%, 70%, 75% and 80% respectively in a series of tests.

During the test, the AE monitoring system should be kept synchronized with the oedometer system. The 2/4/6 preamplifiers were used, and the typical input parameters of AE acquisition system are listed in Table 2. Before the test starts, the AE monitoring system was checked by conducting the pencil-lead break (PLB) test (Hamstad 2007).

In this research, two key AE parameters of interest are ring-down counts (RDC) and peak frequency. RDC refers to the number of oscillations of the AE signal exceeding the pre-defined voltage threshold within a certain period of time, which can continuously reveal the intensity of cracking or breakage behavior resulting in failure (Dixon et al. 2015; Lei et al. 2004; Yuan and Shi 2018). The peak frequency is defined as the point in the Power Spectrum at which the peak magnitude occurs and acquired by performing a real

time Fast Fourier Transform (FFT) on the waveform associated with the AE hit. This parameter is recognized capable of identifying different types of micro-mechanical behaviors such as particle collision and rearrangement, micro-defect formation and cracking, tensile cracking and shear cracking (Lin et al. 2019; Michlmayr and Or 2014; Ohno and Ohtsu 2010). Since the high-pressure oedometer tests were very time-consuming, the maximum effective normal stress of the experiments fitted with the AE monitoring system was only set to 3,200 kPa in this study.

In order to study the changing trends of the morphological characteristics of calcareous sands during the oedometer tests, the particle size analysis needs to be conducted on all samples before and after the tests by the dynamic image analysis through the Microtrac PartAn<sup>3D</sup> Maxi large particle size and shape analyzer. Based on the analysis, the morphological parameters of equivalent diameter ( $D$ ), aspect ratio ( $\alpha$ ), flatness ( $\beta$ ), sphericity ( $S$ ) and convexity ( $C$ ) can be determined based on the obtained particle length, width, thickness, perimeter, and area. The detailed definitions can be found in our recent publication by Wei et al. (2020).

## Results and discussion

### The influence of initial packing density and particle size

Figure 2a) shows the evolution of void ratio ( $e$ ) with effective normal loading stress ( $p'$ ) for sample of initial relative density from 50 to 80% and particle size range of 2–5 mm during the one-dimensional compression. The evolution pattern can be divided into three stages, namely, the slowly descending stage (stage 1), steep descending stage (stage 2) and approximate linear stage (stage 3). In state 1, the compression pressure was lower than 400 kPa. In this stage, the loading stress on the sand sample was not very high and the sample was gradually consolidated. Meanwhile, the void ratios decreased slowly because of the resistance from the particle interlocking and internal friction. The steep descending stage had the loading pressure of 400 and 3000 kPa. With the increase of the loading stress, the sample void ratio reduced rapidly. In stage 3 (beyond yield, i.e., the point of maximum curvature on the curves), the void ratios decreased approximately linearly with the increase of loading stress. The compression curves of sand samples with different relative densities converged to the limiting compression curve (LCC) as proposed by Pestana and Whittle (1995). At high loading stresses, the void ratios became extremely low. This value appeared to be dependent on the particle size but independent on sample relative density. For samples with the same particle size distribution,

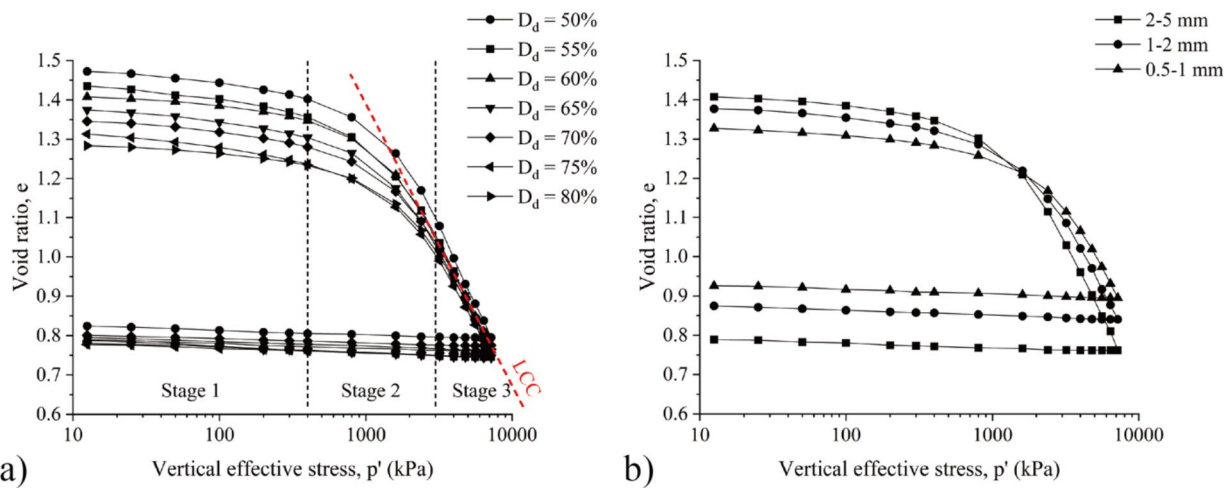


**Fig. 2** One-dimensional compression curves for calcareous sands (a) with different relative densities in the size range of 2–5 mm, (b) in different size ranges with initial relative density of 60%

the compression would finally lead to the same sample void ratio. The variation of the void ratio of the specimen in the unloading phase was very small ( $<0.05$ ), and the  $e - p'$  curve was approximately a straight line.

Figure 2b) presents the  $e - p'$  plots of calcareous sands with the same initial relative density (60%) but different particle size range of 2–5 mm, 1–2 mm, and 0.5–1 mm in the oedometer tests. At the beginning of the test, the initial void ratio of specimen increases with the sizes of constituent particles due to the relatively large pore space between coarse particles. However, the trend reversed when the normal stress exceeded 1600 kPa. This is because intense particle breakages occurred among coarse particles, producing a large number of fine sands which quickly filled the interparticle voids. As a result, a more rapid decrease in the void ratio of the coarse specimen occurred. For samples with fine particles, the decrease in the void ratio was not as fast as that of the coarse ones due to the relatively low particle breakage of fine particles at a dense packing state. Under 7200 kPa, the final void ratio of 2–5 mm sands was smaller than samples with finer particles, because the fine particles generated during the compression have filled up the interparticle pores, resulting in a densely packed sample.

During one-dimensional compression, the yield stress can be used as an indicator of the occurrence of large-scale particle breakage. When the loading stress is less than this value, the crushing is mainly caused by the breaking of smaller asperities or grinding of particle surfaces. However, particle breakage will play a dominate role when the yield stress has been reached (Chuhan et al. 2003; Fernandes et al. 2010). The yield stress can be determined either analytically or graphically. It can be obtained by graphic method proposed by Casagrande (1936) or at the point where the deformation changes the most rapidly (Nakata, Kato, et al. 2001).

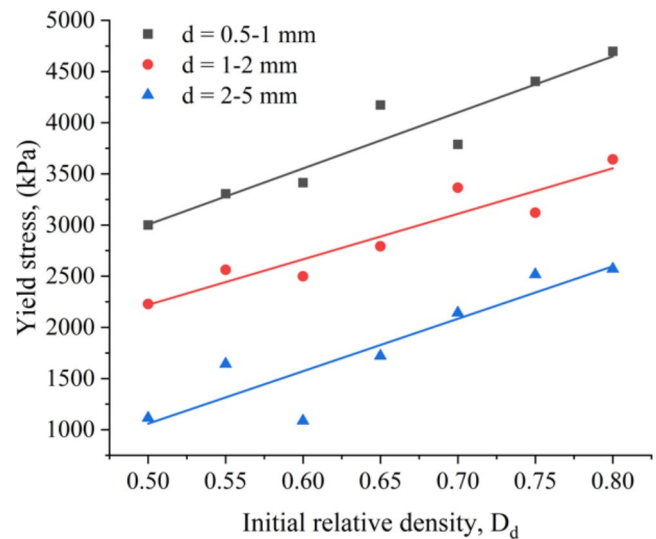


**Fig. 3** The relationships between the yield stress and initial relative density and particle size

McDowell (2002) defined the yield stress as the loading stress at the point of maximum curvature on the void ratio ( $e$ ) - logarithm of effective stress ( $\sigma'$ ) plot for sands subjected to oedometric compression. This method was applied in this study and the results are summarized in Fig. 3.

As illustrated in Fig. 3, as the initial relative density increases, the yield stress of calcareous sands of different particle sizes increases with the relative density, indicating that denser samples can generally resist higher loading stresses before significant particle breakages occur. The yield stress of calcareous sands increases with the decrease of particle size. Therefore, large particles have lower strength than the finer ones because they are more likely to have internal weak zones (e.g., fracture, crack) and have higher coordination numbers (Fonseca et al. 2013).

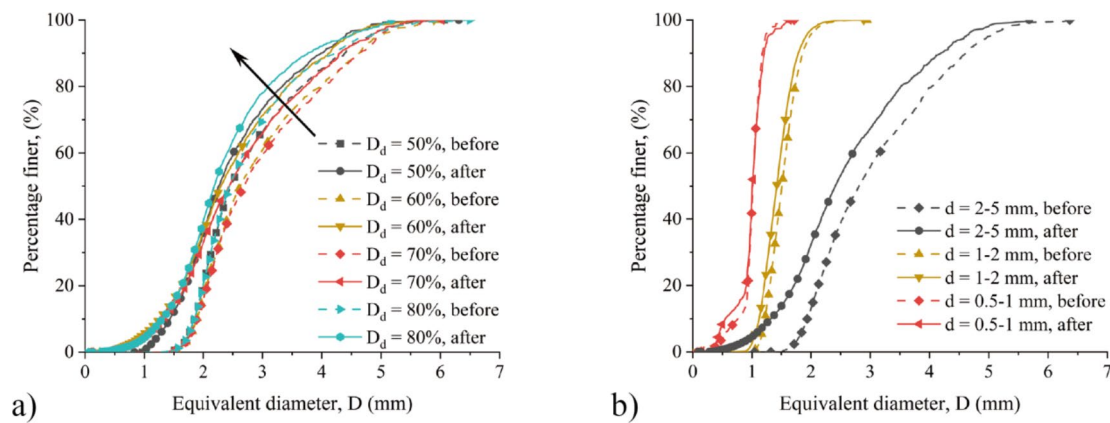


**Fig. 4** Initial (dashed curves) and final (solid curves) gradings of calcareous sand samples. **(a)** Particle size is fixed as 2–5 mm but different initial relative density; **(b)** the initial relative density is fixed as 65%, but different particle sizes

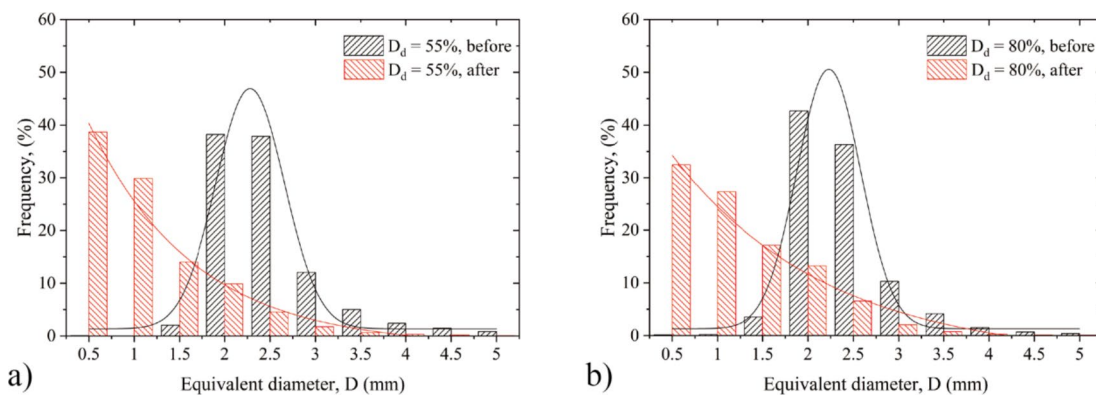


**Fig. 5** Statistics of calcareous sand particles of size of 2–5 mm (by number) before and after the compression with the initial relative density of **(a)** 55% and **(b)** 80%

### Dynamic image analysis

Although the traditional method proposed by Hardin (1985) is one of the most popular ways for calculating the relative particle breakage, there are still some limitations, such as time-consuming and discontinuous particle size. Thus, the calculations are not accurate due to the limited number of data points on particle size distribution curves. Wei et al. (2020) innovatively proposed a quantitative method to determine the particle breakage intensity based on the dynamic image analysis (DIA), which could analyze the PSD results with higher accuracy within a short time. In DIA, the individual particles in the testing samples are firstly scanned by a high-speed camera in the PartAn<sup>3D</sup> Maxi particle size and shape analyzer (Microtrac 2022), and the particle morphologies, e.g., size, shape descriptors, are statistically analyzed by the postprocessing software PartAn<sup>3D</sup>. The measurement principle complies with ISO 13322-2:2021 for dynamic image analysis (ISO 2021). In the analysis, the equivalent particle diameter is defined as the diameter of a circle with the same surface area as the projected particle area. The

total solid volume for particles finer than specific diameter was analyzed.

Fig. 4 a) shows the initial and final gradings of 2–5 mm calcareous sands with different initial relative densities. After the compression, all grading curves shifted in the direction as indicated by the arrow, which means a decrease in the size of large particles and a significant increase of fines. The changes in curve positions for specimens of lower relative densities ( $D_d=50\%$  and  $60\%$ ) were slightly more pronounced than those with higher relative densities ( $D_d=70\%$  and  $80\%$ ), indicating that more intensive particle breakage occurred in the sample with lower relative densities, producing a larger portion of fine particles. Figure 4b) illustrates the influence of particle size on the evolution of PSDs of samples with the same initial relative density ( $D_d=65\%$ ). It is obvious that the larger the particle size, the more obvious the change in its PSD curve. More fine particles generated by the larger samples, indicating that more intensive particle breakage occurred. The 0.5–1 mm sample has negligible change of PSD curve after the test. For coarse sand particles, the irregular shape, surface roughness and

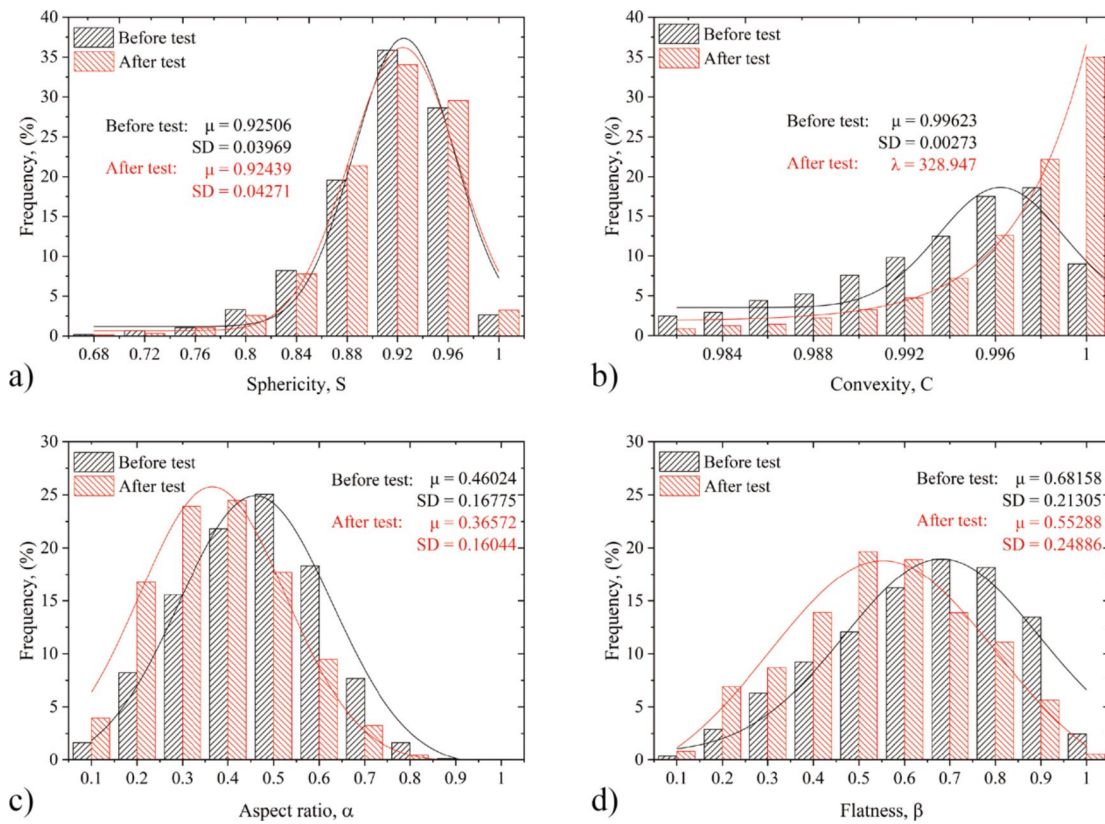


**Fig. 6** Distribution of particle shape descriptors before and after the oedometer test: **(a)** sphericity; **(b)** convexity; **(c)** aspect ratio; and **(d)** flatness

the inner pores make the overall damage of particles more likely to occur.

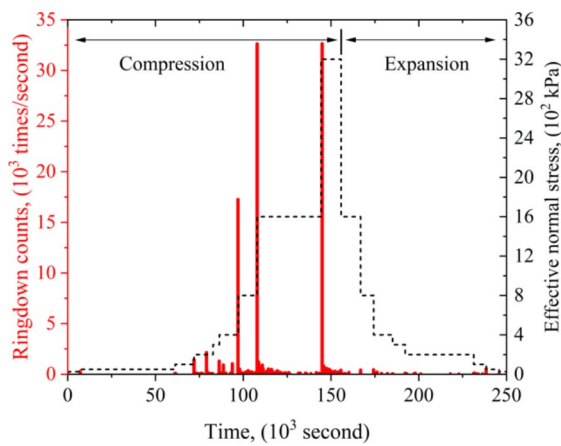
Figure 5 shows the frequency of particle sizes before and after the compression. Before loading, the calcareous sands were uniformly graded, with particle size in the range of 2–5 mm, following a Gaussian distribution pattern (black curves). After the tests, most of the particles (more than 90%) were finer than 2 mm following an exponential distribution, indicating that a large number of calcareous sands have been crushed. The compression has significantly reduced the number of coarse particles in the specimen. Besides, it is obvious that the frequency counts of fine particles (0–0.5 mm) for samples with  $D_d=80\%$  is smaller than that of samples with  $D_d=55\%$ , which confirms that loose samples generate more fine particles than that of dense ones.

Figure 6 presents the statistical frequency of particle shape descriptors for calcareous sands of size 2–5 mm and the initial relative density of 65%. The mean ( $\mu$ ) is the abscissa of the center of the distribution and the standard deviation (SD) is the measure of the variation around the mean. Before loading, the frequency of particle shape descriptor followed well the Gaussian distribution. After the loading-unloading cycles, the frequency of morphological parameters still exhibited the same distribution, except for the convexity which showed an exponential distribution ( $\lambda$

is the rate parameter). The slight decline in  $\mu$  of the particle sphericity indicated that the newly generated particles have more angular shapes (Fig. 6a). After the test, more than 84% particles have the convexity value larger than 0.99 (Fig. 6b), illustrating that the asperity of most particles were worn or damaged, which resulted in smoothed surfaces. The obvious decrease in the mean particle aspect ratio (Fig. 6c) and particle flatness (Fig. 6d) were also observed, illustrating that the produced particles after the tests were more elongated and flatter. The evolution trends in the statistical distribution of the particle shape descriptors demonstrate that the finer particles produced during compression by catastrophic splitting have more elongated and flatter shapes, while the flatter or damage of the asperities can generate smoother particle surfaces.

**AE tests**

To characterize the intensity and distinguish different modes of the micro-mechanical behaviors during oedometer tests, the AE ringdown counts (RDC) and peak frequency were studied respectively. Figure 7 presents the measurements from tests conducted on calcareous sands with particle size range of 1–2 mm and initial relative density of 60% to exemplify the evolutions of RDC and effective normal



**Fig. 7** Evolutions of AE ringdown counts with time during oedometer tests on calcareous sands with particle size range of 1–2 mm and initial relative density of 60%

stress with time. It is exhibited that almost every significant increase in RDC occurred at the moment of loading or reloading under each stress level. The specimen was initially featured by only a few of AE RDC when normal stress was less than 400 kPa (i.e., the stage 1 in Fig. 2a) due probably to particle sliding. AE activity increased significantly under higher stress levels (800 kPa) since the normal stress was high enough to abrade surface asperities and induce micro-cracking. An extremely rapid increase of RDC is observed and the maximum appeared when the normal stress reached its peak as more intensive particle breakage occurred in calcareous sands. Finally, no obvious RDC signals could be detected during the expansion stage since acoustic waves have close relation to irreversible deformations (Lin et al. 2019).

Figure 8 illustrates the influence of initial relative density ( $D_d$ ) and particle size on the evolutions of cumulative AE ringdown counts with effective normal stress. The solid scatter symbols represent the cumulative RDC results during compression, which are best fitted using the logistic

function. Meanwhile, the hollow symbols represent the data obtained during expansion stages and are linear fitted. All the  $R^2$  values are larger than 0.96, indicating good fitting accuracy. It is illustrated that regardless of different  $D_d$  or particle sizes, the evolution of the RDC during all the oedometer tests exhibited a similar trend. A small amount of AE count occurred during the initial loading stages. As the stress increased, the signal count number increased exponentially and appeared to be concentrated in the compression stage of loading stress 400 to 3200 kPa. The AE counts and stress reached the maximum values at the same time. The counting signals of calcareous sands mainly occurred in the compression stage, which can be barely found in the expansion stage. As demonstrated in Fig. 8a), for 1–2 mm calcareous sands, when the normal loading stress was higher than 400 kPa, the observed counting signal of loose samples ( $D_d=60\%$  and  $70\%$ ) increased more rapidly than that of the denser one ( $D_d=80\%$ ) as intense asperity abrasion and particle rearrangement (particle sliding) occurred in loose sands. Under higher loading stresses ( $> 800$  kPa), the dense samples could resist higher loading stresses and a smaller number of sands were crushed. Therefore, less counting signals could be observed. As shown in Fig. 8b), the generation of AE signals during compression were highly dependent on the particle size. Under the same initial relative density ( $D_d=70\%$ ), coarse calcareous sands of size 2–5 mm could generate more AE signals than finer ones, indicating that more significant particle breakage occurred in samples consisting of coarser particles. This is because the coarser particles have more persistent internal defects and surface asperities, which could effectively trigger catastrophic failure. For sands of size 0.5–1 mm, the effects caused by the irregular surface of the finer particles was greatly reduced, and their spatial arrangement has little influence on strength variation. Thus, the particle breakage was more difficult to be initiated, so that the value of RDC is generally small.

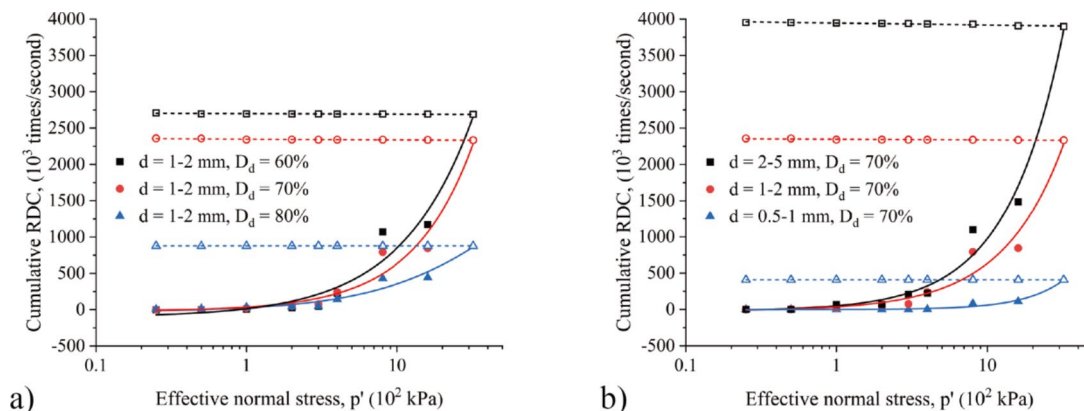


**Fig. 8** Evolutions of cumulative AE ringdown counts of calcareous sands (a) with different relative densities but the same size range as 1–2 mm, (b) in different size ranges but the same initial relative density as 70%



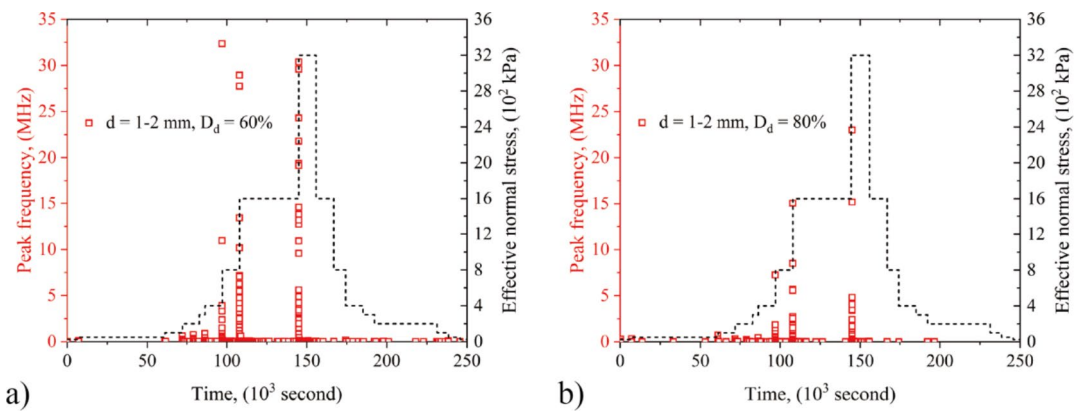


**Fig. 9** Evolutions of AE peak frequency with time during oedometer tests on calcareous sands with particle size of 1–2 mm and initial relative density of (a) 60% and (b) 80%

Figure 9 presents the evolutions of peak frequency of all AE waveforms detected during the whole oedometer tests on calcareous sands with the particle size of 1–2 mm and different initial relative densities, along with the corresponding effective normal stress against time relations. It is illustrated that the AE hits generated under the load less than 800 kPa during both tests are predominated by low-frequency AE components at around 0.02 MHz. In general, particle rearrangement and inter-particle friction are often dominated with low-frequency AE components ( $< 100$  kHz), while particle breakage has a much higher contents ( $> 100$  kHz) (Mao and Towhata 2015). In the initial stage of the test, the instantaneous loading of the normal stress has a certain effect on the specimen. The interparticle voids of the loose specimen are compressed, which generated less low-frequency signals; while the particles of the dense specimen were already in contact with each other, and more particle friction occurred at the moment of load application, and thus more low-frequency signals have been produced. From 800 kPa and upwards, the peak frequency values of loose samples ( $D_d=60\%$ ) increased rapidly and most of which were concentrated approximately in the interval of 0–4, 0–7.5, and 0–15 MHz under the load of 800, 1600 and 3200 kPa, respectively, with the maximum value of approximately 32.5, 29 and 30 MHz. However, as presented in Fig. 9b), both the high-frequency range and its maximum value of the denser specimen decreased significantly. It seems that the rapid decrease of high-frequency AE components is closely related to the reduction in occurrence of particle breakage since that denser samples can generally resist higher loading stresses and limit the particle breakage (Lin et al. 2019; Muñoz-Ibáñez et al. 2019). In addition, a decrease in the low-frequency components indicates that particle sliding was inhibited in denser packed samples.

## Conclusion

This research studied the soil deformation and quantified the morphology of individual calcareous sands by oedometer tests. A normal loading pressure up to 7200 kPa was applied on samples consisting of sands in different particle size ranges and different initial relative densities. The particle breakage, morphology evolution and AE signal characteristics were illustrated and explained.

1. The compression of calcareous sands with different initial relative densities results in NCL of the same inclination due to particle breakage. Both the particle size and initial relative density affect the compression and breakage of calcareous sand. The quantity of particle breakage of calcareous sands increases with the particle size and the decrease of the initial relative density. The yield stress of calcareous sands is approximately in the range of 1 to 4.7 MPa and increases with the particle size and the decrease of the particle size.
2. The DIA results showed that the distribution frequency of particle sphericity, convexity, aspect ratio and flatness before tests followed well the Gaussian distribution pattern. After oedometer tests, the produced fine particles tended to more spherical, elongated and flatter with smoother surfaces.
3. The compressive deformation and breakage of calcareous sands are consistent with the AE characteristics, regardless of different particle size ranges or initial relative density. The AE ringdown counts (RDC) and peak frequency of the associated acoustic waveforms could better reflect the intensity and type of AE-triggering micro-mechanical behaviors, respectively. The AE ringdown counts signal concentrated primarily in the compression phase and increased significantly under the normal stress of 400–3200 kPa. The values increased with the increase of particle size but decreased with

the increase of initial relative density. Particle sliding (rearrangement) is a dominant process throughout the compression stage, which generates lower frequency AE components (at around 0.02 MHz), while high-frequency components (up to 30 MHz) are considered closely related to particle breakage.

**Acknowledgements** This research was supported, in whole or in part, by the *National Natural Science Foundation of China* (grant Nos. 41877260 and 41877267), *UK Engineering and Physical Sciences Research Council (EPSRC) New Investigator Award* (grant EP/V028723/1), and the open funding of the State Key Laboratory of Geomechanics and Geotechnical Engineering (No. Z019004). A CC BY or equivalent licence is applied to that at least the Author Accepted Manuscript (AAM) arising from this submission, in accordance with the grant's open access conditions.

## Declarations

**Conflict of interest statement** All authors disclosed no relevant relationships.

**Open Access** This article is licensed under a Creative Commons Attribution 4.0 International License, which permits use, sharing, adaptation, distribution and reproduction in any medium or format, as long as you give appropriate credit to the original author(s) and the source, provide a link to the Creative Commons licence, and indicate if changes were made. The images or other third party material in this article are included in the article's Creative Commons licence, unless indicated otherwise in a credit line to the material. If material is not included in the article's Creative Commons licence and your intended use is not permitted by statutory regulation or exceeds the permitted use, you will need to obtain permission directly from the copyright holder. To view a copy of this licence, visit <http://creativecommons.org/licenses/by/4.0/>.

## References

- Alba J, Audibert J (1999) Pile design in calcareous and carbonaceous granular materials, and historic review, The 2nd International Conference on Engineering for Calcareous Sediments. sn, pp. 29–44
- Altuhafi F, Coop MR (2011) Changes to particle characteristics associated with the compression of sands. *Géotechnique* 61:459–471
- Ata A, Salem TN, Hassan R (2018) Geotechnical characterization of the calcareous sand in northern coast of Egypt. *Ain Shams Engineering Journal* 9:3381–3390
- Bandini V, Coop MR (2011) The influence of particle breakage on the location of the critical state line of sands. *Soils Found* 51:591–600
- Bolton M, Cheng Y (2002) Micro-geomechanics. Constitutive and centrifuge modelling: Two extremes (ed. SM Springman), 59–74
- Brandes H (2011) Simple shear behavior of calcareous and quartz sands. *Geotech Geol Eng* 29:113–126
- Casini F, Viggiani GM, Springman SM (2013) Breakage of an artificial crushable material under loading. *Granular Matter* 15:661–673
- Chuhan FA, Kjeldstad A, Bjørlykke K, Høeg K (2003) Experimental compression of loose sands: relevance to porosity reduction during burial in sedimentary basins. *Can Geotech J* 40:995–1011
- Coop M, Lee I (1992) The behaviour of granular soils at elevated stresses, *Predictive soil mechanics: Proceedings of the Wroth Memorial Symposium held at St Catherine's College, Oxford, 27–29 July 1992*. Thomas Telford Publishing, pp. 186–198
- Coop M, Sorensen K, Bodas Freitas T, Georgoutsos G (2004) Particle breakage during shearing of a carbonate sand. *Géotechnique* 54:157–163
- Dixon N, Spriggs M, Smith A, Meldrum P, Haslam E (2015) Quantification of reactivated landslide behaviour using acoustic emission monitoring. *Landslides* 12:549–560
- El Aal AA, Nabawy BS (2019) Implications of increasing the ferruginous cement on the physical and mechanical properties of the Cambro-Ordovician Wajid Sandstone in southwest Saudi Arabia: applications for construction purposes. *Bull Eng Geol Environ* 78:817–836
- Fernandes F, Syahrial AI, Valdes JR (2010) Monitoring the oedometric compression of sands with acoustic emissions. *Geotech Test J* 33:410–415
- Fonseca J, O'Sullivan C, Coop MR, Lee P (2013) Quantifying the evolution of soil fabric during shearing using directional parameters. *Géotechnique* 63:487–499
- Hagerty M, Hite D, Ullrich C, Hagerty D (1993) One-dimensional high-pressure compression of granular media. *J Geotech Eng* 119:1–18
- Hamstad MA (2007) Acoustic emission signals generated by monopole (pencil lead break) versus dipole sources: finite element modeling and experiments. *J Acoust Emission* 25:92–106
- Hardin BO (1985) Crushing of soil particles. *J Geotech Eng* 111:1177–1192
- Hardin BO (1987) 1-D strain in normally consolidated cohesionless soils. *J Geotech Eng* 113:1449–1467
- He H, Li S, Senetakis K, Coop MR, Liu S (2021) Influence of anisotropic stress path and stress history on stiffness of calcareous sands from western Australia and the Philippines. *Journal of Rock Mechanics and Geotechnical Engineering*
- Hyodo M, Wu Y, Kajiyama S, Nakata Y, Yoshimoto N (2017) Effect of fines on the compression behaviour of poorly graded silica sand. *Geomech Eng* 12:127–138
- Jardine R, Zhu B, Foray P, Yang Z (2013) Measurement of stresses around closed-ended displacement piles in sand. *Géotechnique* 63:1–17
- Karatza Z, Andò E, Papanicolopulos S-A, Viggiani G, Ooi JY (2019) Effect of particle morphology and contacts on particle breakage in a granular assembly studied using X-ray tomography. *Granular Matter* 21:44
- Kikumoto M, Wood DM, Russell A (2010) Particle crushing and deformation behaviour. *Soils Found* 50:547–563
- Lei X, Masuda K, Nishizawa O, Jouniaux L, Liu L, Ma W, Satoh T, Kusunose K (2004) Detailed analysis of acoustic emission activity during catastrophic fracture of faults in rock. *J Struct Geol* 26:247–258
- Li G, Ovalle C, Dano C, Hicher P-Y (2013) Influence of grain size distribution on critical state of granular materials. *Constitutive modeling of geomaterials*. Springer, pp 207–210
- Lin W, Liu A, Mao W (2019) Use of acoustic emission to evaluate the micro-mechanical behavior of sands in single particle compression tests. *Ultrasonics* 99:105962
- Liu L, Liu H, Xiao Y, Chu J, Xiao P, Wang Y (2018) Biocementation of calcareous sand using soluble calcium derived from calcareous sand. *Bull Eng Geol Environ* 77:1781–1791
- Luzzani L, MR C (2002) On the relationship between particle breakage and the critical state of sands. *Soils Found* 42:71–82
- Ma G, Zhou W, Chang X-L (2014) Modeling the particle breakage of rockfill materials with the cohesive crack model. *Comput Geotech* 61:132–143
- Ma G, Zhou W, Chang X-L, Yuan W (2014) Combined FEM/DEM modeling of triaxial compression tests for rockfills with polyhedral particles. *Int J Geomech* 14:04014014

- Manso J, Marcelino J, Caldeira L (2018) Crushing and oedometer compression of rockfill using DEM. *Comput Geotech* 101:11–22
- Mao W, Towhata I (2015) Monitoring of single-particle fragmentation process under static loading using acoustic emission. *Appl Acoust* 94:39–45
- McClelland B (1988) Calcareous sediments: an engineering enigma, International conference on calcareous sediments, pp. 777–784
- McDowell G (2002) On the yielding and plastic compression of sand. *Soils Found* 42:139–145
- McDowell G, Amon A (2000) The application of Weibull statistics to the fracture of soil particles. *Soils Found* 40:133–141
- McDowell G, Bolton M (1998) On the micromechanics of crushable aggregates. *Géotechnique* 48:667–679
- McDowell G, Bolton M, Robertson D (1996) The fractal crushing of granular materials. *J Mech Phys Solids* 44:2079–2102
- McDowell G, Harireche O (2002) Discrete element modelling of soil particle fracture. *Géotechnique* 52:131–135
- Mesri G, Vardhanabhuti B (2009) Compression of granular materials. *Can Geotech J* 46:369–392
- Miao G, Airey D (2013) Breakage and ultimate states for a carbonate sand. *Géotechnique* 63:1221–1229
- Michlmayr G, Or D (2014) Mechanisms for acoustic emissions generation during granular shearing. *Granular Matter* 16:627–640
- Mun W, McCartney JS (2017) Roles of particle breakage and drainage in the isotropic compression of sand to high pressures. *J Geotech GeoEnviron Eng* 143:04017071
- Muñoz-Ibáñez A, Delgado-Martín J, Grande-García E (2019) Acoustic emission processes occurring during high-pressure sand compaction. *Geophys Prospect* 67:761–783
- Murff JD (1987) Pile capacity in calcareous sands: state of the art. *J Geotech Eng* 113:490–507
- Nabawy BS, El Aal AA (2019) Impacts of the petrophysical and diagenetic aspects on the geomechanical properties of the dolomitic sequence of Gebel El-Halal, Sinai, Egypt. *Bull Eng Geol Environ* 78:2627–2640
- Nabawy BS, Ibrahim E, Kahal A, Alfaihi HJ, Lashin AA (2020) Impact of authigenic iron oxides, clay content and grain size on the aquifer quality properties of the Cambrian-Ordovician Wajid Sandstone, southwest Saudi Arabia. *J Afr Earth Sc* 172:104000
- Nakata Y, Hyodo M, Hyde AF, Kato Y, Murata H (2001) Microscopic particle crushing of sand subjected to high pressure one-dimensional compression. *Soils Found* 41:69–82
- Nakata Y, Kato Y, Hyodo M, Hyde AF, Murata H (2001) One-dimensional compression behaviour of uniformly graded sand related to single particle crushing strength. *Soils Found* 41:39–51
- Ohno K, Ohtsu M (2010) Crack classification in concrete based on acoustic emission. *Constr Build Mater* 24:2339–2346
- Pestana JM, Whittle A (1995) Compression model for cohesionless soils. *Géotechnique* 45:611–631
- Pino LFM, Baudet BA (2015) The effect of the particle size distribution on the mechanics of fibre-reinforced sands under one-dimensional compression. *Geotext Geomembr* 43:250–258
- Randolph M, Gourvenec S (2017) *Offshore geotechnical engineering*. CRC press
- Russell AR, Khalili N (2004) A bounding surface plasticity model for sands exhibiting particle crushing. *Can Geotech J* 41:1179–1192
- Sadrekarimi A (2012) Effect of soil particle mineralogy on embankment dams. *Proceedings of the Institution of Civil Engineers-Geotechnical Engineering* 165, 195–206
- Salem M, Elmamlouk H, Agaiby S (2013) Static and cyclic behavior of North Coast calcareous sand in Egypt. *Soil Dyn Earthq Eng* 55:83–91
- Shi D, Zheng L, Xue J, Sun J (2016) DEM modeling of particle breakage in silica sands under one-dimensional compression. *Acta Mech Solida Sin* 29:78–94
- Uygar E, Doven AG (2006) Monotonic and cyclic oedometer tests on sand at high stress levels. *Granular Matter* 8:19–26
- Wang G, Wang Z, Ye Q, Wei X (2020) Particle breakage and deformation behavior of carbonate sand under drained and undrained triaxial compression. *Int J Geomech* 20:04020012
- Wang W, Coop M (2016) An investigation of breakage behaviour of single sand particles using a high-speed microscope camera. *Géotechnique* 66:984–998
- Wang X, Wang X-Z, Zhu C-Q, Meng Q-S (2019) Shear tests of interfaces between calcareous sand and steel. *Mar Georesources Geotechnology* 37:1095–1104
- Wei H, Li X, Zhang S, Zhao T, Yin M, Meng Q (2021) Influence of particle breakage on drained Shear Strength of Calcareous Sands. *Int J Geomech* 21:04021118
- Wei H, Zhao T, Meng Q, Wang X, Zhang B (2020) Quantifying the morphology of Calcareous Sands by dynamic image analysis. *Int J Geomech* 20:04020020
- Wils L, Van Impe P, Haegeman W (2015) One-dimensional compression of a crushable sand in dry and wet conditions, 3rd International Symposium on Geomechanics from Micro to Macro. Taylor and Francis Group-London, pp. 1403–1408
- Wood DM, Maeda K (2008) Changing grading of soil: effect on critical states. *Acta Geotech* 3:3
- Wu Y, Yamamoto H, Cui J, Cheng H (2020) Influence of load mode on particle crushing characteristics of silica sand at high stresses. *Int J Geomech* 20:04019194
- Xiao Y, Liu H (2017) Elastoplastic constitutive model for rockfill materials considering particle breakage. *Int J Geomech* 17:04016041
- Xiao Y, Liu H, Chen Q, Ma Q, Xiang Y, Zheng Y (2017) Particle breakage and deformation of carbonate sands with wide range of densities during compression loading process. *Acta Geotech* 12:1177–1184
- Xiao Y, Liu H, Chen Y, Jiang J (2014) Strength and deformation of rockfill material based on large-scale triaxial compression tests. I: influences of density and pressure. *J Geotech GeoEnviron Eng* 140:04014070
- Xiao Y, Sun Z, Desai CS, Meng M (2019) Strength and surviving probability in grain crushing under acidic erosion and compression. *Int J Geomech* 19:04019123
- Xiao Y, Wang L, Jiang X, Evans TM, Stuedlein AW, Liu H (2019) Acoustic emission and force drop in grain crushing of carbonate sands. *J Geotech GeoEnviron Eng* 145:04019057
- Xiao Y, Yuan Z, Chu J, Liu H, Huang J, Luo S, Wang S, Lin J (2019) Particle breakage and energy dissipation of carbonate sands under quasi-static and dynamic compression. *Acta Geotech* 14:1741–1755
- Xu D-s, Huang M, Zhou Y (2020) One-Dimensional Compression Behavior of Calcareous Sand and Marine Clay Mixtures. *Int J Geomech* 20:04020137
- Yao T, Baudet BA, Lourenço SD (2022) Evolution of surface roughness of single sand grains with normal loading. *Géotechnique* 72:543–555
- Yu F (2017) Particle breakage and the critical state of sands. *Géotechnique* 67:713–719
- Yu F (2018) Particle breakage and the undrained shear behavior of sands. *Int J Geomech* 18:04018079
- Yuan R, Shi B (2018) Acoustic emission activity in directly tensile test on marble specimens and its tensile damage constitutive model. *Int J Coal Sci Technol* 5:295–304
- Zhang C, Yang Z, Nguyen G, Jardine R, Einav I (2014) Theoretical breakage mechanics and experimental assessment of stresses surrounding piles penetrating into dense silica sand. *Géotechnique* Lett 4:11–16
- ASTM. Standard Practice For Classification Of Soils For Engineering Purposes (Unified Soil Classification System), *West Conshohocken, ASTM D2487-17* (2018).

Nanjing Ningxi Soil Instrument Co., Ltd.. Single lever consolidation instrument (triple high pressure), *Nanjing Ningxi Soil Instrument Co., Ltd.*, [Product 122](#) (2022).

Microtrac. Particle size and shape analyzer PARTAN 3D, *Microtrac*, [Dynamic Image Analysis PARTAN 3D](#) (2022).

MISTRAS Group. MICRO-II – COMPACT PCIAE CHASSIS, *Physical Acoustics*, [Micro-II](#) (2022).

ISO. Particle size analysis — Image analysis methods — Part 2: Dynamic image analysis methods, *ISO*, [ISO 13322-2:2021](#) (2021).

**Publisher's Note** Springer Nature remains neutral with regard to jurisdictional claims in published maps and institutional affiliations.